Diagnosis of Shell-Core Mixing Using Absorption and Emission Spectra of a Doped Layer

A major limitation on fusion target performance is the mixing of shell material with the fuel during the final stage of the implosion. This mixing is the result of hydrodynamic instabilities that cause nonuniformities on the inner surface of the shell to grow as the shell decelerates. The seeds for this growth are nonuniformities that grow sufficiently during the acceleration phase to feed through the shell. This acceleration-driven growth is initially seeded by laser and target nonuniformities. The open geometry of planar targets has been used extensively to investigate growth during acceleration; however, to study deceleration-driven growth and shell-core mixing, implosions are required.[1] Recent experiments used the image of x-ray emission from the shell (enhanced by high-Z doping) to diagnose these effects experimentally.[2] We have subsequently shown theoretically[3] that when backlighter imaging is used in the experiment, additional information is obtained and the ability to detect shell-core mixing is enhanced. We have also shown[3–5] that in such a backlighting experiment, monochromatic imaging (using, for example, a diffracting crystal) is required because of the overwhelming self-emission from the target.

We present here the analysis of a different diagnostic method for detecting shell-core mixing that does not require backlighting; in effect, the central core emission is used as a backlighter for the surrounding shell. A particular target experiment is simulated and the expected experimental signature calculated and analyzed. This signature is the emerging x-ray spectrum rather than the target image, as was the case in the work cited above. The absorption spectrum produced when the core radiation traverses an embedded signature layer in the shell was reported earlier.[6] In that work (conducted in collaboration with LANL), we showed that when a KCl layer is embedded in a CH shell that is imploded as an exploding pusher, the continuum core radiation produces absorption lines of K and Cl ions that provide information on the temperature and $\rho\Delta r$ of the imploded shell. Here we show that, in doped targets that suffer shell-core mixing, emission lines of the dopant ions can appear due to inward migration of doped material. We show that for OMEGA experiments a small admixture of titanium dopant in a thin CH layer is sufficient for the measurement of titanium lines, yet creates minimal perturbation of the target behavior. We calculate the emerging spectra of a particular target implosion on the OMEGA laser. For this test case, *LILAC* results were used for the expected temperature and density profiles of the unmixed target. A post-processor code was developed[4] to calculate the emission and transport through the target. A simple procedure is used to simulate the mixing, and the radiation transport equation is then solved for unmixed as well as mixed targets.

The target is a polymer shell of 940-μm diameter and 30-μm thickness, filled with 80 atm DT gas. Within the CH polymer shell is a layer doped with titanium; the doped-layer thickness and position within the shell are varied. The concentration of titanium atoms, 1% by atom number, is such that a doped layer of a few-micron initial thickness would show significant absorption at the wavelengths of titanium lines. One-dimensional simulations by *LILAC* showed that the addition of such a layer made little change in hydrodynamic behavior. (This point is discussed further in the next section.) The choice of titanium was dictated by the fact that, at peak compression of the test target, radiation wavelengths shorter than ~3 Å are needed to avoid severe continuum absorption by the shell (as opposed to the much stronger line absorption). On the other hand, too high a Z (and thus too short wavelengths) would cause even the line absorption, essential to the method, to be insignificant.

For all simulations, the laser pulse is trapezoidal, rising linearly over 0.1 ns to 13.5 TW, then remaining constant for 2.2 ns, before dropping linearly over 0.1 ns. Figure 65.14 shows the density and electron-temperature profiles predicted for this target at peak compression. The shell material has been compressed to a mean radius of ~50 μm and a thickness of ~30 μm, with a density in the range of ~10 to 50 g/cm^3, corresponding to a $\rho\Delta r$ value of ~90 mg/cm^2. The electron temperature in the shell ranges from ~80 to ~800 eV. Most of the line absorption will occur within the colder, outer part of this compressed shell.

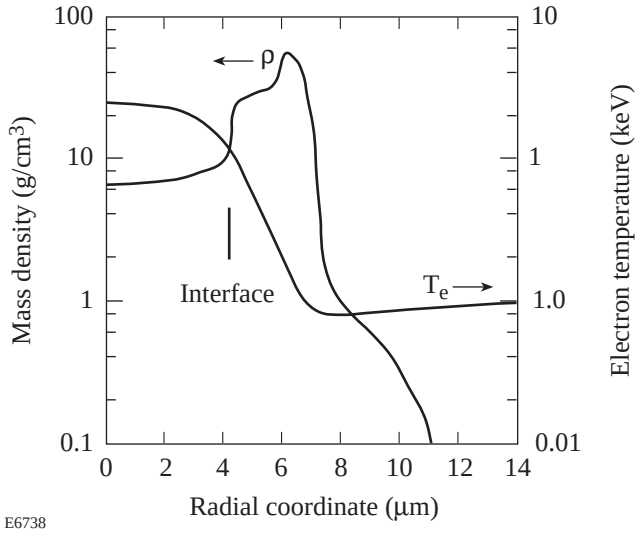

Figure 65.14
The density and electron-temperature profiles predicted by the *LILAC* code at peak compression for the case studied in this article. The vertical bar marks the position of the shell-fuel interface.

Modeling of Target Mixing and Radiation Transport

The procedure for modeling shell-core mixing was described in an earlier publication.[3] This procedure is applied to *LILAC*-calculated profiles of a particular implosion experiment; it does not include self-consistent feedback, i.e., the effect of mixing in one time step upon the hydrodynamics and radiation physics in subsequent steps. The limitations resulting from this simplification will be discussed. Briefly, mixing occurs during the deceleration (or burn) phase of the implosion. The model determines a radial region within which mixing is assumed to occur, the width of which is characterized by a parameter α. It is defined such that the deepest penetration of shell material into the fuel region spans a fraction α of the distance between the shell-core interface radius and the free-fall line (defined as the constant-velocity trajectory at the shell maximum velocity). As time progresses, this penetration increases; however, for the α values considered here, the penetration is not severe enough to reach the target center. Simulations of Rayleigh-Taylor unstable implosions[7] show that, in the nonlinear regime of the instability, the shell penetrates into the fuel in the form of spikes; between the spikes, the fuel penetrates into the shell region in the form of bubbles whose penetration is typically half that of the spikes (for an Atwood number close to 1). Within the mixed region, the fuel and shell material densities are assumed to decay linearly into each other's region. As explained in Ref. 3, this choice is more realistic than a uniformly mixed region. In particular, the resulting fraction of, say, fuel material as part of the total density is reasonably smooth and reaches the correct values at the boundaries of the mixed region. Furthermore, the effect of the mixing on the temperature and electron density distributions in the mixed region was also included. Finally, the model allows for the mixing of specific doped layers; namely, the dopant material follows the CH element in which it was embedded initially, and the percentage of doping remains the same.

To discern whether the discontinuity introduced by the doping increases any existing instability and thus mixing, the influence of doping on the growth rate of Rayleigh-Taylor instability was investigated. We note that the linear growth rate is proportional to $A^{1/2}$, where A is the Atwood number, defined as $(\rho_h - \rho_l)/(\rho_h + \rho_l)$ in terms of the high and low mass densities on each side of the discontinuity. In our case the density discontinuity caused by the doping is 2%, which by itself would give rise to an Atwood number of $A \sim \Delta\rho/2\rho \sim 0.01$. In typical target implosions, the Atwood number (determined by the density gradients near the ablation surface) is in the range of 0.5 to 1.0;[7,8] it can therefore be estimated that the growth-rate increase due to doping is less than 10%.

To simulate the emergent absorption and emission spectra, multigroup opacity tables were generated using the OPLIB opacity library.[9] The radiation transport model developed earlier[4] was used to calculate the emergent spectra. That model uses temperature and density profiles generated by *LILAC* and the multigroup opacity tables to calculate radiation emission and absorption. The use of the OPLIB opacity calculations requires the assumption of LTE conditions, the applicability of which is discussed in the following section.

Figures 65.15 and 65.16 show examples of OPLIB data for two density and two temperature values, relevant to the conditions of Fig. 65.14. The spectra consist of helium-like and hydrogen-like lines, including satellite lines that appear on the low-energy side of those lines. The major difference between the spectra at $T = 0.4$ keV and $T = 1$ keV is the appearance of the hydrogen-like (Lyman) lines; this is because, at the lower temperature, the population of the hydrogen-like specie is negligibly small. In going from a density of 0.4 to 12.8 g/cm^3, the plasma becomes less ionized, as indicated by a lower relative intensity of the Lyman lines when comparing the two $T = 1$ keV curves (the Lyman lines are absent from the lower temperature curves). Also, a comparison of the satellite manifold near the He-α line (especially for the two $T = 0.4$ keV

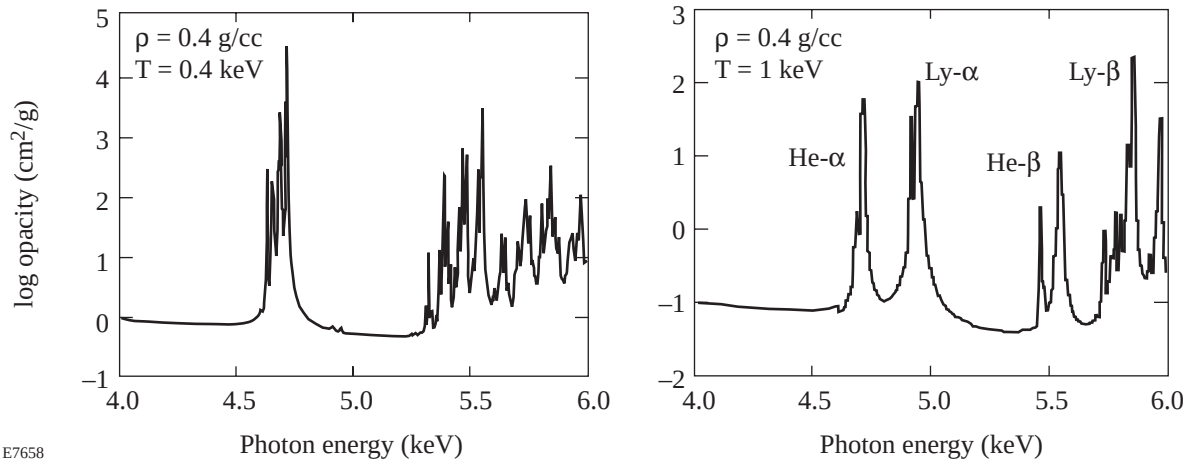

Figure 65.15
Examples of OPLIB opacity data for CH polymer containing 1% titanium (by number of atoms) for a density of 0.4 g/cm^3, at two temperatures.

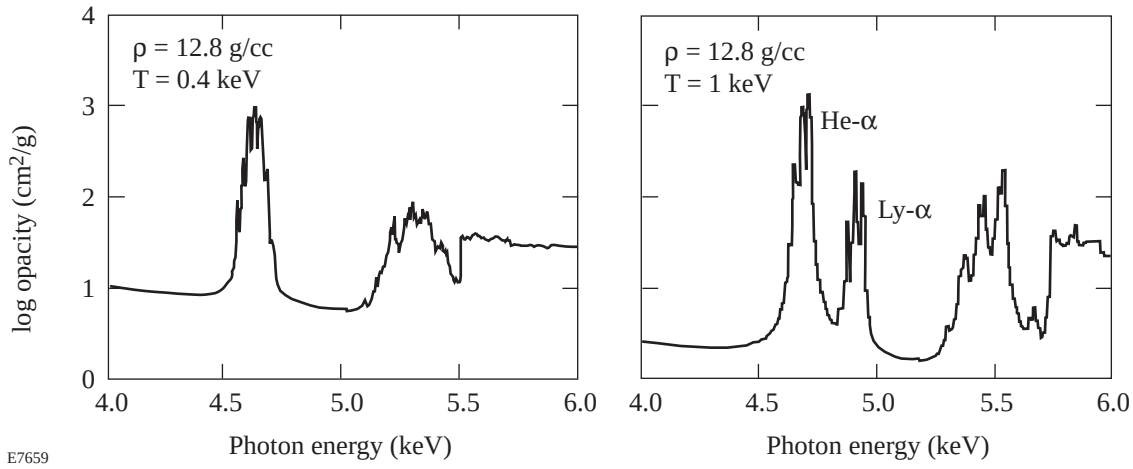

Figure 65.16
Examples of OPLIB opacity data for CH polymer containing 1% titanium (by number of atoms) for a density of 12.8 g/cm^3, at two temperatures.

curves) shows an intensity distribution of the peaks that is skewed more toward high energies for the lower-density case, again indicating decreased ionization with increasing density. This is the result of the increasing importance of three-body recombination, which rises faster with density than other, two-body processes. In the case for $T = 0.4$ keV and $\rho = 12.8$ g/cc, the combined effect of the low temperature and high density reduces the ionization to the point where even the He-α line is hardly visible. In that case, the spectrum consists mostly of satellite lines. Finally, we note that the absolute magnitude of the opacity tends to increase with increasing density and to decrease with increasing temperature, but these trends are modified by the changes in line ratios discussed above.

Satellite lines appear on the low-energy side of the various lines, such as the He-α line (at 4.7495 keV), the Lyman-α line (at 4.9733 keV), the He-β line (at 5.5821 keV), and the Lyman-β line (at 5.8915 keV). The satellite lines correspond to transitions similar to that of the nearby resonance line, in ion species that are progressively less ionized. For example, the He-α line corresponds to the transition $1s2p\ ^1P$–$1s^2\ ^1S$, whereas those of the nearby satellites correspond to transitions

of the type $1s(2l)^m$–$1s^2(2l)^{m-1}$, where m changes from 2 (Li-like specie) to 8 (F-like specie). Since the satellite lines correspond to L-shell ions, they are excited in colder target regions as compared with those of the K-shell ions. This is the basis for the mixing diagnostics described next.

Target Design for Mixing Diagnostics

The diagnostic method for mixing relies on the sharp temperature gradient at the shell-fuel interface within the imploded shell (see Fig. 65.14). Near that interface, the temperature is high enough (~0.5 to 1.0 keV) for the emission of helium-like and hydrogen-like titanium K-shell lines. In this method, the titanium layer is placed in the original target far enough from the interface, such that in a stable target, it never gets hot enough to significantly emit these lines. Then, mixing causes migration of doped polymer into the high-temperature regions closer to the fuel interface, thus causing emission of these lines.

Having chosen the doping material and concentration, we next determine the optimal location of the doped layer within the fabricated target. Figure 65.17 shows the spectra calculated using the OPLIB opacity tables and the radiation transport model described above, using the target profiles of Fig. 65.14 (peak compression in an unmixed target). A signature layer at different locations within the shell consists of 1% titanium doping (by atom number) in the CH polymer. The boundaries of the signature layer in the initial target, with respect to the shell-core interface, are (a) 0 to 1.12 μm, (b) 0.9 to 1.12 μm, (c) 0.92 to 1.12 μm, and (d) 0.94 to 1.12 μm. The continuous spectrum emitted by an undoped target is also shown. The curves represent the x-ray fluence per unit area along a line of sight through the center of the target (with unit magnification), normalized to a spectral intensity of 7.0×10^{20} keV/(keV ns cm^2 Ω).

Each spectrum shown in Fig. 65.17 contains two distinct features: (a) the absorption-line manifold in the range ~4.5 to 4.7 keV, and (b) the higher-energy emission lines. Feature (a) consists of satellite lines near the He-α line. These lines are absorbed within the colder, outer part of the compressed shell, as is evidenced by the fact that they are almost identical when comparing the four spectra of Fig. 65.17. The ionization energy of the Li-like to F-like species ranges from ~1.4 keV down to ~0.8 keV. These species will predominate in regions of temperatures lower than ~0.5 keV. Figure 65.14 shows that the temperature of the outer half of the compressed shell is indeed within this range; it is there that these satellite lines are absorbed. It should be noted that these satellite lines usually appear in absorption but not in emission. The temperature where species with $n = 2$ bound electrons can exist is insufficient for exciting $n = 1$ electrons. Thus, the satellite lines can be excited only by continuum radiation streaming from higher-temperature regions, leading to absorption lines at energies that are at resonance with satellite transitions. However, these lines can appear in emission in flat-target experiments[10] since

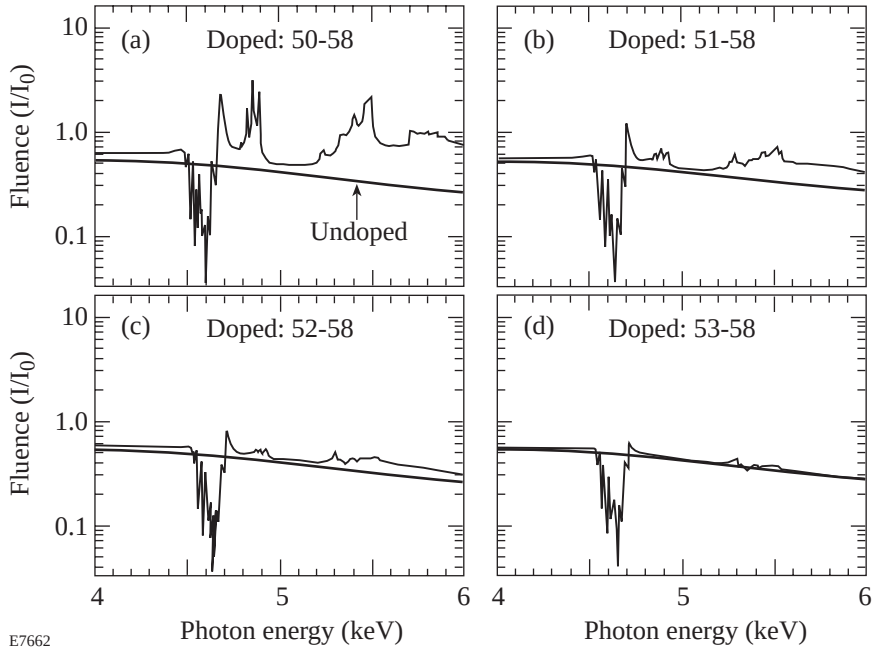

Figure 65.17
Predicted spectrum, at the time of peak compression, emitted by the imploded target of Fig. 65.14, with no mixing. A signature layer is added at different locations within the shell (Lagrangian code zone numbers are shown). The boundaries of the signature layer in the initial target, with respect to the shell-core interface are (a) 0 to 1.12 μm, (b) 0.9 to 1.12 μm, (c) 0.92 to 1.12 μm, and (d) 0.94 to 1.12 μm. The continuous spectrum due to an undoped target is also shown. The curves represent the target fluence per unit area along a line of sight through the center of the target (at the plane of the target), normalized to a spectral intensity of 7.0×10^{20} keV/(keV ns cm^2 Ω).

the exciting continuum is then moving into the target, and the detector sees only the fluorescent lines emitted as a consequence of the radiative excitation.

The spectral lines above ~4.7 keV (from helium-like and hydrogen-like ions) are seen in Fig. 65.17 to be emitted only close to the interface, where the temperature is sufficiently high to excite these lines. One may wonder why these lines are not seen to be absorbed far from the interface. The helium-like and hydrogen-like lines could be absorbed in regions where the temperature is sufficiently high to ionize all $n = 2$ electrons but not high enough to excite these lines; evidently the region of this intermediate temperature is too narrow for significant absorption.

The various features in Fig. 65.17 offer the possibility of diagnosing mixing: if the doped layer is placed as in the target of Fig. 65.17(d), the spectrum in the absence of mixing will show only the absorption lines in the range of ~4.5 to 4.7 keV. However, mixing could cause some of the titanium material to migrate to hotter regions, which will cause the appearance of emission lines in the range above 4.7 keV [as in Fig. 65.17(a)].

The titanium concentration should be high enough to yield substantial line absorption but low enough to minimize its effect on the target behavior. Figure 65.17 shows significant line absorption (attenuation by up to a factor of ~10) on the lines in the range of 4.5 to 4.7 keV. The minimal effect on the target behavior is evidenced by the negligible increase in continuum emission with respect to the no-doping case. The considerations for optimizing the doped-layer location within the fabricated target are as follows: The inner radius of the doped region should be far enough removed from the interface to show no emission of lines in the absence of mixing, yet not too far so as to require very severe mixing to yield a difference in the spectrum. Figure 65.17(d) shows an optimal choice for this distance. Finally, the outer radius of the doped layer should extend far enough from the interface to give rise to significant line absorption, otherwise the dopant concentration must be increased. The extent of the layer must be limited to minimize the effects on the stability of the ablating part of the target.

The applicability of the LTE assumption in using the OPLIB opacity library will be discussed in this section, in view of the spectra shown in Fig. 65.17. Generally speaking, the LTE approximation becomes valid for high-density, low-temperature, and low-nuclear-charge conditions. Note that the two groups of lines in the titanium spectrum originate from different ion species (see Fig. 65.17): absorption lines come from lower ionizations (Li-like to O-like species) and emission lines come from higher ionizations (He-like and H-like). We examined the equilibrium conditions for these two line groups separately (following Ref. 11) for the compressed-shell conditions in Fig. 65.14. The condition for complete LTE [Eq. (6-60) in Ref. 11] for a temperature of 300 eV and average excitation energy of 1 keV is that ρ be greater than ~7 g/cm^3. For the L-shell species giving rise to the absorption lines (Fig. 65.17), the condition is well satisfied for the compressed shell. It should be emphasized that the assumption of LTE is not critical when calculating the spectrum of absorption lines. Absorption lines depend on the ground-state populations that are almost equal to the total density of the pertinent ion specie, whereas, emission lines depend on the excited-state populations that can vary greatly between LTE and non-LTE model predictions. Furthermore, the absorption manifold observed in the spectrum corresponds to a range of ion species of successive ionizations. Therefore, small deviations from LTE would merely redistribute some of the absorption among neighboring ionic features, but the total amount of absorption will hardly change. Turning to the emission lines, we find by comparison with results obtained with the non-LTE code *POPION*[12] that the LTE model slightly overestimates the intensity of He-like lines and greatly overestimates that of the H-like lines. Thus, in comparing experimental spectra to theoretical results, emphasis should be placed on the helium-like lines.

Effect of Mixing on the Spectrum

We apply now the mixing model described earlier to the target experiment under consideration (Fig. 65.14) and calculate the emergent spectrum for various degrees of mixing. As mentioned, the portion of the CH layer from 0.94 μm to 1.12 μm away from the interface was doped with titanium at a concentration of 1% by atom number.

Figures 65.18 and 65.19 show the results of such calculations for two mixing severities: $\alpha = 0.2$ and $\alpha = 0.4$, respectively. The curve marked "undoped" corresponds to an undoped and unmixed target simulation that is shown as a reference. The mixing in the case $\alpha = 0.2$ (Fig. 65.18) is seen to be too weak to be diagnosed using the emitted spectrum. The main effect of mixing on the spectrum in Fig. 65.18 is a slight lowering of the intensity in the emergent continuum. This occurs because mixing causes the transfer of some titanium material to smaller radii, thus increasing its areal density ($\rho\Delta r$) and increasing the absorption of the core continuum by the titanium in the shell.

When the mixing level is increased to $\alpha = 0.4$, the effect, as seen in Fig. 65.19, is dramatic. For clarity, the curves for the

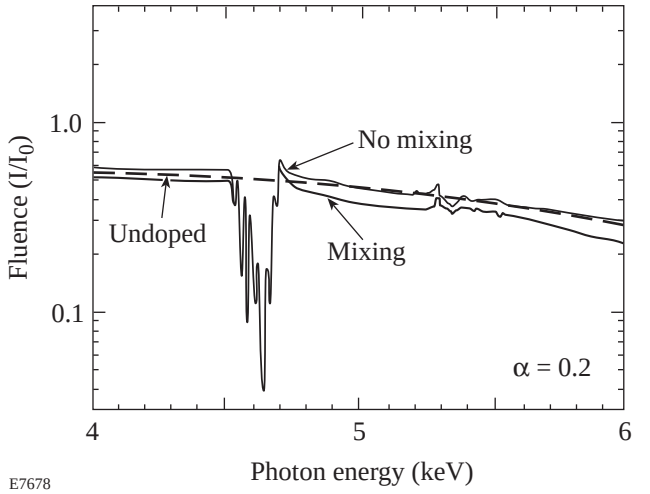

Figure 65.18
Effect of mixing on the spectrum shown in Fig. 65.17(d), for a mixing parameter $\alpha = 0.2$. The profiles of the absorption line manifold for the two cases essentially overlap. The curve marked "undoped" corresponds to an undoped as well as unmixed target run.

case of mixing and for the case of no mixing are shown separately, and on different scales, in Figs. 65.19(a) and 65.19(b). Mixing causes the level of the emitted continuum to rise because some of the titanium migrates into the high-temperature layer close to the interface. However, the main mixing signature is the appearance of emission lines above ~4.7 keV. More quantitatively, mixing can be indicated by the measured ratio of emission to absorption lines, for which only relative line intensities need to be measured. As seen in Fig. 65.19, the absorption-line manifold does not change appreciably due to mixing. Since the absorption of these titanium lines (relative to the continuum level) depends[6,13] mainly on the $\rho\Delta r$ of cold doped layer, this indicates that the $\rho\Delta r$ is not reduced appreciably due to the transfer of some cold doped material into the hot interface region. The appearance of this absorption manifold in the measured spectrum can thus serve to determine how much of the cold shell remained intact in spite of mixing.

The emission lines above 4.7 keV include helium-like and hydrogen-like lines, as well as satellites near the Lyman-α line and the He-β line. These latter satellites do not appear in absorption, as do the satellites near the He-α line, for the following reasons: The satellites near the Lyman-α line are due to transitions of the type $2p2l$–$1s2l$, so that the absorbing level $1s2l$ is an excited state; thus, the density of ions that can absorb these transitions is relatively small. On the other hand, satellites near the helium-like lines are absorbed by ions in ground configurations, $1s^2 2l$, whose relative density is high.

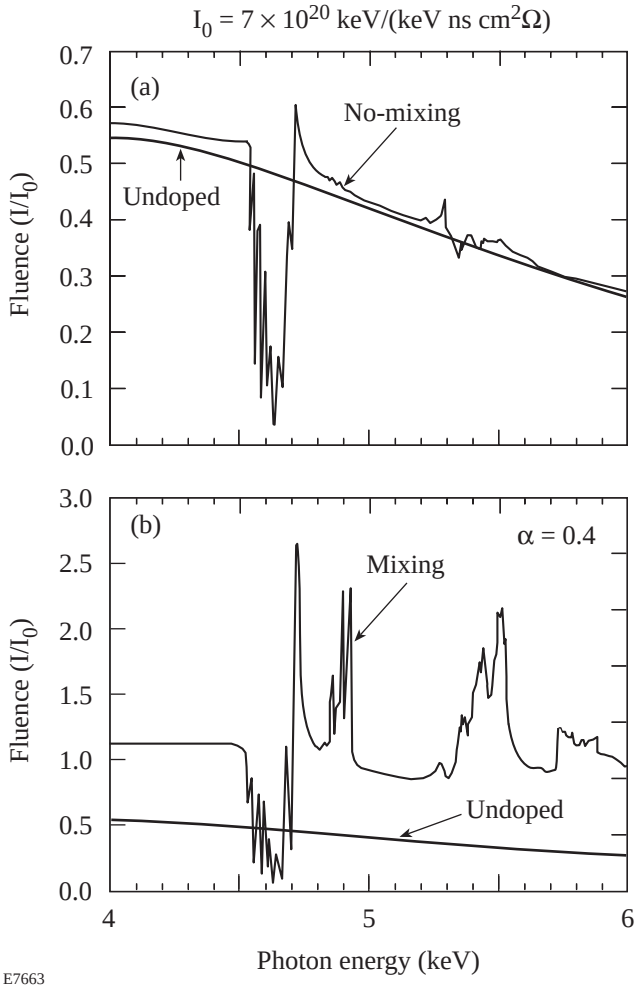

Figure 65.19
Effect of mixing (b) on the spectrum (a) from Fig. 65.17(d), for a mixing parameter $\alpha = 0.4$. The curve marked "undoped" corresponds to an undoped as well as unmixed target run.

The $\rho\Delta r$ of the absorption region is apparently high enough to absorb the satellite lines near the He-α line but not to absorb the weaker satellite lines near the He-β line (the latter, however, have previously been observed in absorption in argon[13]). In comparing the line absorption in Fig. 65.19(a) to that in Fig. 65.19(b), one would have expected less absorption in the latter case because the transfer of some titanium to the high-temperature layer necessarily reduces the amount of cool, absorbing titanium. However, the relative absorption in the two cases is comparable because some titanium moves inward but still remains within the absorbing layer, yielding a higher areal density of absorbing material.

We compare this method with a similar mixing experiment involving chlorine-doped, argon-filled targets.[14] Both meth-

ods are based on the observation of spectral lines of a shell dopant that moves into higher-temperature regions due to mixing. In the Cl/Ar method, the use of relative line intensities from the two elements obviates the need for absolute intensity measurement; here, a similar role is played by the comparison of emission and absorption lines. Generally, the choice of dopant has to be adjusted to the expected conditions: a higher-Z dopant is required to probe higher temperatures and to escape from higher-compression targets.

We finally consider an experiment based on the results presented here. Since the determination of mixing relies on comparison with code simulations, we have to allow for uncertainties in the modeling. In particular, results such as in Figs. 65.18 and 65.19 do not account for self-consistent hydrodynamic calculations. Thus, the core temperature can be expected to rise less if the compression is unstable. This effect would reduce the intensity of emitted titanium lines and counter the intensity rise due to mixing. To address this concern, the experiment should include a normalizing target, where the doping extends up to the interface [as in Fig. 65.17(a)]. We show in Fig. 65.20 the effect of mixing at a level of $\alpha = 0.4$ on such a doped target. As seen, the effect is minor since the interface contains doped material even without mixing. The line emission from this target is therefore dependent mostly on the core temperature rather than on mixing and can serve as a normalizing experiment. For example, if an experiment using the target of Fig. 65.17(a) shows strong line emission, but one using the target of Fig. 65.17(d) does not, we can surmise that the mixing is smaller than $\alpha = 0.4$ since the interface is hot enough for the emission of titanium lines. This assumes that the cooling effect of the instability on the two targets is comparable. This is to be expected since, as shown for the present level of doping, the effect on target energetics is small. More quantitatively, we can calculate the intensity ratio between emitted titanium lines in Fig. 65.19(b) and in Fig. 65.20(b) as a function of α. This ratio depends strongly on α since only the former case depends strongly on mixing; the latter is seen to be almost independent of mixing [by comparing Figs. 65.20(a) and 65.20(b)]. Self-consistent modeling would cool the core about equally in the two cases since the target energetics depend mostly on the mixing, not the doping.

The calculation results shown in Figs. 65.18 and 65.19 correspond to an axial view of the target at peak compression. To realize these conditions in the experiment, a spatially resolving slit should be placed in front of the spectrometer. Since the diameter of the core at peak compression in Fig. 65.14 is ~50 μm, the slit width need not be much narrower than that. To limit the measurement to the peak of the compression, the spectrum should be detected with a streak or framing camera; however, since most of the radiation from imploding targets such as in Fig. 65.14 is emitted around peak compression, a time-integrating instrument should also provide useful results.

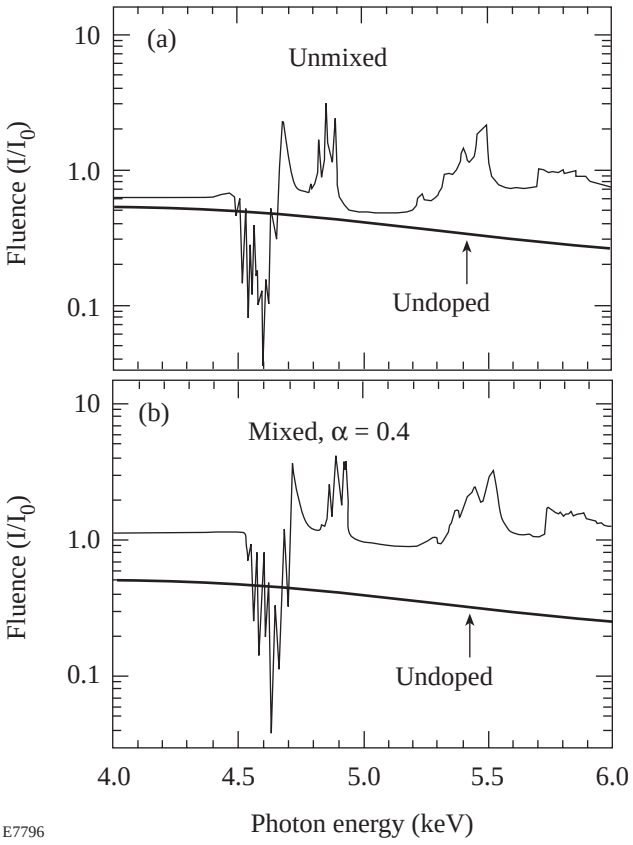

Figure 65.20
Effect of mixing on the spectrum shown in Fig. 65.17(a), for a mixing parameter $\alpha = 0.4$. The curve marked "undoped" corresponds to an undoped as well as unmixed target run.

ACKNOWLEDGMENT

This work was supported by the U. S. Department of Energy Office of Inertial Confinement Fusion under Cooperative Agreement No. DE-FC03-92SF19460, the University of Rochester, and the New York State Energy Research and Development Authority. The support of DOE does not constitute an endorsement by DOE of the views expressed in this article.

REFERENCES

1. J. D. Lindl, R. L. McCrory, and E. M. Campbell, Phys. Today **45**, 32 (1992).

2. O. L. Landen, W. K. Levendahl, and T. R. Dittrich, Bull. Am. Phys. Soc. **38**, 2083 (1993).

3. Laboratory for Laser Energetics LLE Review **59**, NTIS document No. DOE/SF/19460-36, 1994 (unpublished), p. 114 .

4. Laboratory for Laser Energetics LLE Review **58**, NTIS document No. DOE/SF/19460-17, 1994 (unpublished), p. 57.

5. B. Yaakobi, F. J. Marshall, Q. Su, and R. Epstein, J. X-Ray Sci. Technol. **5**, 73 (1995).

6. A. Hauer, R. D. Cowan, B. Yaakobi, O. Barnouin, and R. Epstein, Phys. Rev. A **34**, 411 (1986).

7. C. P. Verdon, R. L. McCrory, R. L. Morse, G. R. Baker, D. I. Meiron, and S. A. Orszak, Phys. Fluids **25**, 1653 (1982).

8. D. L. Youngs, Physica **12D**, 32 (1984); S. W. Haan, Phys. Rev. A **39**, 5812 (1989); N. Freed, D. Ofer, D. Shvarts, and S. A. Orszag, Phys. Fluids A **3**, 912 (1991).

9. M. F. Argo and W. F. Huebner, J. Quant. Spectrosc. Radiat. Transfer **16**, 1091 (1976).

10. B. Yaakobi, J. Delettrez, L. M. Goldman, R. L. McCrory, W. Seka, and J. M. Soures, Opt. Commun. **41**, 355 (1982).

11. H. R. Griem, in *Plasma Spectroscopy* (McGraw-Hill, New York, 1964), Chap. 6.

12. R. Epstein, S. Skupsky, and J. Delettrez, J. Quant. Spectrosc. Radiat. Transfer **35**, 131 (1986).

13. B. Yaakobi, R. Epstein, F. J. Marshall, D. K. Bradley, P. A. Jaanimagi, and Q. Su, Opt. Commun. **111**, 556 (1994).

14. T. R. Dittrich *et al*., Phys. Rev. Lett. **73**, 2324 (1994).